Finite-Element Evaluations of Geogrid-Reinforced Asphalt Overlays over Flexible Pavements

N. S. Correia, Ph.D.[1]; E. R. Esquivel, Ph.D.[2]; and J. G. Zornberg, Ph.D., F.ASCE[3]

Abstract: Geosynthetics have been extensively implemented as a pavement maintenance solution to minimize reflective cracking. However, geosynthetics within asphalt overlays can also be used to improve the pavement structural capacity, potentially resulting in reduced permanent displacements and strains in pavement structural layers. Combination of accelerated pavement testing techniques and numerical simulations would be particularly suitable to assess the comparatively new use of geogrids for increased structural capacity of asphalt overlays. Accordingly, this study focuses on two-dimensional finite-element simulations conducted to identify the variables that govern the performance of geogrid-reinforced asphalt overlays and their effect on the response of flexible pavements. The finite-element model is validated by comparing the numerical predictions with the experimental results obtained in large-scale accelerated paved models. A series of finite-element parametric evaluations is conducted by varying the stiffness of both the geogrid and the subgrade materials. The strains mobilized within the geogrid under static loading are also evaluated. The numerical predictions indicate that the presence of the geogrids significantly affects the structural behavior of the pavement, as observed through reduced vertical displacements and strains, although such reductions are not significantly affected by the increases in geogrid stiffness. A reduction in pavement stresses is observed, mainly in the base course layer. The finite-element parametric evaluations show that geogrids placed within the asphalt layers are able to increase the overall bearing capacity of the pavement system, even for cases involving weak subgrades. Finally, the mechanisms of structural enhancement can be associated with numerically predicted geogrid strain distribution, which is found to be particularly consistent with experimental results. **DOI: [10.1061/JPEODX.0000043](https://doi.org/10.1061/JPEODX.0000043).** © 2018 American Society of Civil Engineers.

Author keywords: Pavement modeling; Finite element; Asphalt overlay; Geogrid; Reinforcement.

Introduction

New materials and technologies have made road design, construction, and maintenance more sustainable and resilient, and new methods facilitate determining when, where, and how best to preserve pavements (ASCE 2017). As a new technology, geosynthetics have been extensively implemented to minimize reflective cracking in paved roads (Austin and Gilchrist 1996; Khodaii et al. 2009; Gonzalez-Torre et al. 2015). More recently, geogrids have been considered as reinforcement inclusions in asphalt overlays to improve the mechanical performance of newly constructed or rehabilitated pavements (e.g., Laurinavičius and Oginskas 2006; Siriwardane et al. 2010; Solaimanian 2013; Graziani et al. 2014; Mounes et al. 2014; Correia and Zornberg 2016). Although relevant, the research conducted on the use of geogrids to structurally enhance asphalt overlays, through both large-scale laboratory and field sections, has been limited. However, the actual data have shown not only that geogrids lead to asphalt tensile strain reductions, but that they minimize permanent displacements and

pavement critical strains. On the other hand, few numerical predictions have been conducted to extrapolate the field and experimental evidence collected so far.

Studies aimed at understanding the reinforcement mechanisms of geosynthetic-reinforced asphalt pavements have been conducted recently, which are expected to aid in the development of mechanistic–empirical design methods (Correia and Zornberg 2016). Pavement performance depends on a significant number of factors, including the mechanical properties and thickness of roadway layers, position, type and properties of the geosynthetic, load characteristics, and the bond between geosynthetic and pavement layers (Taherkhani and Jalali 2016). The effect of combinations of these many factors is difficult to assess through large-scale laboratory or field sections, which can effectively assess only a limited combination of the many parameter values and boundary conditions that may influence the pavement response.

Numerical evaluations using two-dimensional (2D) finite-element simulations have been conducted to assess the mechanical improvement of paved or unpaved road structures using geosynthetic-stablished base courses (e.g., Perkins 2001; Nazzal et al. 2010; Abu-Farsakh and Chen 2011). Numerical simulations have also been reported to assess the mechanical improvement of geosynthetic-reinforced asphalt layers (Pandey et al. 2012; Abu-Farsakh et al. 2014; Faheem and Hassan 2014; Al-Jumaili 2016; Taherkhani and Jalali 2016), but only a few numerical predictions were validated from experimental evidence (Ling and Liu 2003; Abdesssemed et al. 2015).

Some of these studies have aimed at understanding the influence of geogrids positioned at the bottom of the asphalt concrete layer and at different types of loading conditions. Using two-dimensional PLAXIS axisymmetric finite-element simulations, Pandey et al. (2012) analyzed the response of a geogrid-reinforced asphalt

[1]Professor, Dept. of Civil Engineering, Federal Univ. of Sao Carlos, Sao Carlos, CEP 13565-905, Sao Paulo, Brazil (corresponding author). ORCID: https://orcid.org/0000-0002-6867-9596. Email: ncorreia@ufscar.br

[2]Professor, Dept. of Geotechnical Engineering, Univ. of Sao Paulo at Sao Carlos, Sao Carlos, 13566-590, Sao Paulo, Brazil. Email: esquivel@sc.usp.br

[3]Professor, Dept. of Civil Engineering, Univ. of Texas at Austin, Austin, TX 78712. Email: zornberg@mail.utexas.edu

© ASCE 04018020-1 J. Transp. Eng., Part B: Pavements

J. Transp. Eng., Part B: Pavements, 2018, 144(2): 04018020

overlays subjected to static and cyclic loads. They reported that the use of geogrid led to a 14% reduction in asphalt tensile stains under cyclic loading and a reduction of 22% under static loading. Faheem and Hassan (2014) reported the results of 2D PLAXIS simulations to analyze the behavior of geogrid-reinforced asphalt overlays subjected to static and cyclic loadings. A significant improvement of the pavement behavior was observed, as quantified by reduced vertical displacements and effective stresses in the wheel load area. The effect of dynamic loading frequency was found to be significant only for high-amplitude loads, whereas the effect of the geogrid stiffness was found not to affect significantly the pavement mechanical response.

Taherkhani and Jalali (2016) evaluated the effectiveness of the geosynthetics to reduce critical strains in flexible pavements under various dynamic axle load levels and using geogrids stiffness of different values, using ABAQUS. Geogrids (installed at the bottom of asphaltic layer) were mostly effective in reducing asphalt tensile strains, but did not affect the compressive strains achieved in the subgrade. Furthermore, decreasing asphalt tensile strains and compressive strains in the subgrade were found to occur with the use of geogrids.

Al-Jumaili (2016) reported the performance of geogrid-reinforced pavements using three-dimensional (3D) PLAXIS axisymmetric simulations to assess the influence of the geogrid position under cycling loadings. The pavement mechanical response was significantly affected when adding the geogrid between asphalt concrete layers.

In their research on reinforced asphalt concrete pavements, Ling and Liu (2003) described a 2D PLAXIS plane strain finite-element evaluation validated by comparison with results obtained from a series of large-scale pavement models (Ling and Liu 2001). The geogrid was positioned at the interface of the base and the asphaltic layer under monotonic loading. The reinforcement effect was more pronounced for comparatively weaker bases, and increased as the strain level increased in relation to the tensile strain mobilized in the geogrid. Abdesssemed et al. (2015) compared the field monitoring results from a project involving asphalt rehabilitation of a runway airport with the predictions from 3D finite-element simulations conducted using ABAQUS under static loading. The experimental results involving geogrid-reinforced asphalt concrete tensile strains and pavement stresses compared well with the numerical predictions, with dispersions below 10%.

In summary, a review of previous studies involving finite-element evaluations of geogrid-reinforced asphalt overlays reveals the potential benefits of using numerical predictions to assess the impact of geogrids on the pavement mechanical behavior. However, previous studies have not focused on identifying the actual mechanisms that lead to improved pavement performance when using geogrids. In particular, the prediction of tensile strains mobilized in the reinforcements are expected to be particularly useful to achieve this goal. Consequently, this study conducted 2D finite-element simulations to assess the effect of geogrid-reinforced asphalt overlays on the response of flexible pavements, with particular emphasis on assessing the geogrid strain distribution. The numerical simulations were conducted using PLAXIS and were validated by comparing the numerical predictions with the experimental results obtained in large-scale accelerated paved models (Correia 2014). A series of finite-element parametric evaluations was conducted by varying the stiffness of both geogrid and subgrade materials in order to extend the range of properties considered in the experimental program. Simulations also focused on cases involving foundation materials of particularly low shear strength in order to assess the potential of using geogrids embedded in asphalt layers for weak subgrade conditions.

Brief Description of Laboratory Paved Road Model

The results obtained from a series of well-controlled large-scale paved model tests by Correia (2014) were used to validate the finite-element procedures in this research. The large-scale paved road models were loaded using a wheel tracking facility aimed at simulating a truck wheel load. The wheel tracking facility was installed over a large steel testing box with internal dimensions of 1.8 m (height), 1.6 m (width), and 1.8 m (length) where the paved road models were constructed. The wheel (546 mm in diameter and 154 mm in width) resulted in a contact pressure of approximately 700 kPa. The wheel moved at a speed of 3.6 km/h with a load frequency of 0.4 Hz. Correia and Zornberg (2016) provided additional details about the wheel tracking facility, load application, scope of the experimental program, and the instrumentation plan used in this research.

Fig. 1 shows the experimental geogrid-reinforced paved road model setup. The pavement structure consisted of a 60-mm-thick asphalt overlay, a 50-mm asphalt layer, a 200-mm granular base course layer, and a 1.0-m-deep subgrade soil layer. The asphalt concrete (AC) layer was compacted in single lifts using a vibratory plate. The aggregate used for the base course layer (basaltic crushed stones) was classified as A-1-a according to ASTM D3282 (ASTM 2015) and was compacted using 100-mm-thick lifts, also using a vibratory plate. The subgrade layer material was classified as A-7-5 according to ASTM D3282 (ASTM 2015), and it was compacted in the testing box in 50-mm-thick lifts using manual procedures. The target dry density and water content used during construction corresponded to a relatively weak subgrade condition, characterized by a California bearing ratio (CBR) of 4.5%. The geogrid reinforcement involved a polyvinyl alcohol (PVA) geogrid bonded to a polypropylene (PP) nonwoven geotextile, which was installed between the existing asphalt layer and the new overlay. The geogrid reinforcement was characterized by an ultimate tensile strength of 50 kN/m and a secant stiffness of 900 kN/m at 2% strain, according to ASTM D6637 (ASTM 2015). Correia (2014) provided additional details regarding material properties, compaction procedures, and quality control during construction of the paved road models.

An instrumentation program was designed to monitor the relevant variables in the paved road models with the objective of quantifying the mechanical response of the pavement layers under wheel loading. Specifically, asphalt surface vertical displacements were monitored using LVDTs. In addition, H-type asphalt strain gauges (ASG) were installed within the AC layers to measure traffic-induced tensile strains. Finally, pressure cells were installed to monitor vertical stresses at critical locations, such as the interface between AC layers, the bottom of lower AC layer, the middle of the base course, and the top of the subgrade. The strains along the geogrid were measured using mechanical extensometers (Correia 2014).

Finite-Element Validation Using Experimental Results

A 2D axisymmetric finite-element model was developed using the PLAXIS version 8 finite-elements software package (Brinkgreve and Vermeer 1998) to validate numerical predictions against experimental data from large-scale geosynthetic reinforced pavement models. Accordingly, the finite-element model adopted the geometry and mechanical characteristics of one of the large-scale geogrid-reinforced paved road models (Correia 2014) described in Fig. 1. Linear elastic materials were considered for the geogrid and asphalt layer materials. The elastic model was deemed adequate

© ASCE   04018020-2   J. Transp. Eng., Part B: Pavements

J. Transp. Eng., Part B: Pavements, 2018, 144(2): 04018020
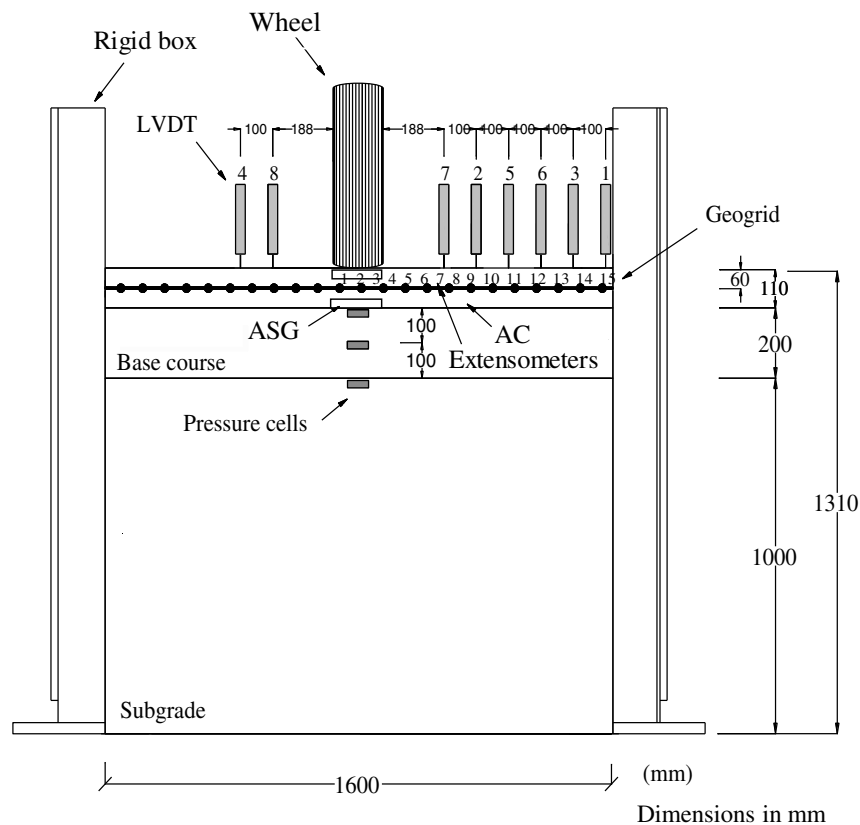
Fig. 1. Experimental geogrid-reinforced paved road model setup.

Table 1. Material properties adopted in numerical simulations

Material	Upper AC surface	Bottom AC surface	Base course	Subgrade
Constitutive model	Linear elastic	Linear elastic	Mohr–Coulomb	Mohr–Coulomb
Thickness	60 mm	50 mm	200 mm	1,000 mm
Unit weight	25 kN/m^3	25 kN/m^3	22 kN/m^3	18 kN/m^3
Young's modulus	2,500 MPa	2,500 MPa	100 MPa	10 MPa
Poisson's ratio	0.35	0.35	0.30	0.40
Cohesion	—	—	0.01 kPa	46 kPa
Friction angle	—	—	45°	26°

considering that the induced strains are very small and considered within the elastic range (Dondi 1994; Perkins 2001; Ling and Liu 2003; Pandey et al. 2012; Faheem and Hassan 2014; Abdesssemed et al. 2015; Al-Jumaili 2016; Taherkhani and Jalali 2016). The geogrid was modeled as structural element with 900 kN/m stiffness defined using the unit tension at 2% axial strain. The base course and the subgrade soils were modeled using the Mohr–Coulomb constitutive model, calibrated using the results from triaxial compression tests (Correia 2014). The selection of this model is consistent with that reported in previous studies (e.g., Ling and Liu 2003; Faheem and Hassan 2014; Al-Jumaili 2016). Table 1 lists the material properties and constitutive models adopted in the initial finite-element simulation.

Fig. 2 shows the 2D finite-element mesh, with 15-noded structural solid elements, used in the analysis of the geogrid-reinforced paved road models. Because of symmetry, only half of the pavement system was simulated. The two sides of the mesh were fixed horizontally but allowed to move vertically, whereas the bottom of the mesh was assumed to be rough by restraining horizontal and vertical displacements. The interaction between the geosynthetic

and asphalt layers was simplified by assuming full bonding between these two layers. This approach was adopted by other researchers (Ling and Liu 2003; Rota 2011; Pandey et al. 2012). The loading condition was simulated in this study by applying a contact pressure of 700 kPa, which was also used in the laboratory tests. Regarding the loading mode, Faheem and Hassan (2014) verified that dynamic loading had no significant influence on the geogrid-reinforced pavement behavior for low stress amplitudes. Other studies investigated the impact of static loads by comparing numerical predictions with dynamic loads in laboratory or field sections (Ling and Liu 2003; Siriwardane et al. 2010; Abdesssemed et al. 2015).

The results obtained from the numerical predictions were compared with experimental results in order to validate the numerical model. Specifically, the rest of this section compares the experimental and predicted effective vertical stress distribution in pavement layers, the asphalt surface displacement profile, and the geogrid strain distribution.

The developed finite-element model accurately predicted the effective vertical stresses measured in the instrumented paved road

© ASCE   04018020-3   J. Transp. Eng., Part B: Pavements

J. Transp. Eng., Part B: Pavements, 2018, 144(2): 04018020
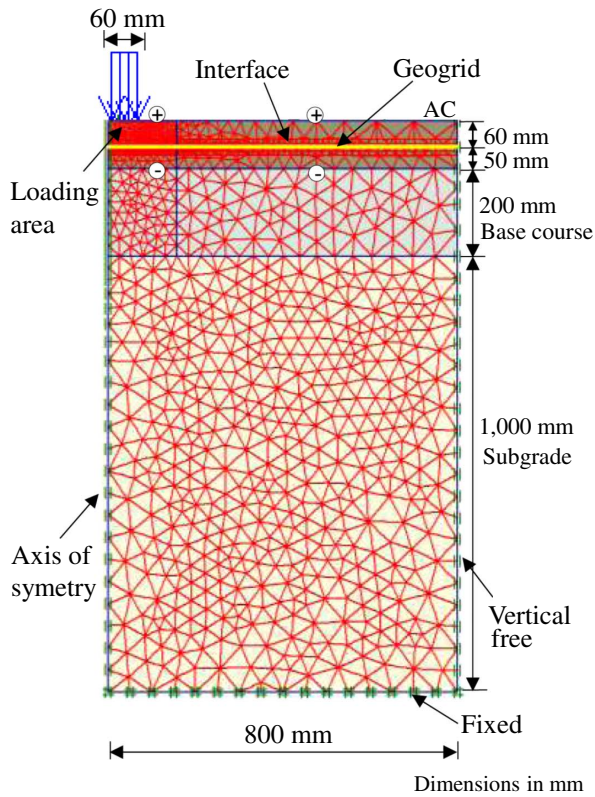
Fig. 2. 2D finite-element meshed geogrid-reinforced paved road model.

model (Fig. 3). The good comparison was observed for all the considered critical locations (at the interface between asphalt layers, at the bottom of lower asphalt layer, in the middle of the base course, and 10 cm below the top of the subgrade layer). Fig. 4 compares the experimental and predicted final rutting profile (i.e., surface vertical displacement). In this case, too, the finite-element model was capable of accurately simulating the maximum vertical displacements under the wheel load area (rutting) obtained in the laboratory paved road model. However, the numerical predictions do not show the AC upheaval area alongside wheel track that is observed in the experimental results. The excessive deformation in the experimental results can be explained by an initial asphalt concrete consolidation, which is commonly characterized by postcompaction phase (Paterson 1987). As indicated in the
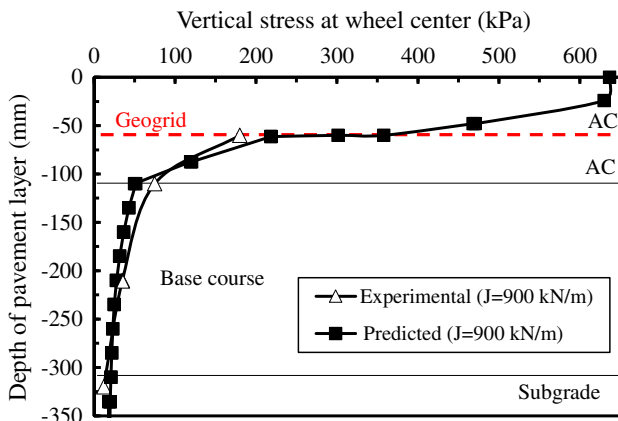
Fig. 3. Comparison of experimental and predicted vertical stresses.
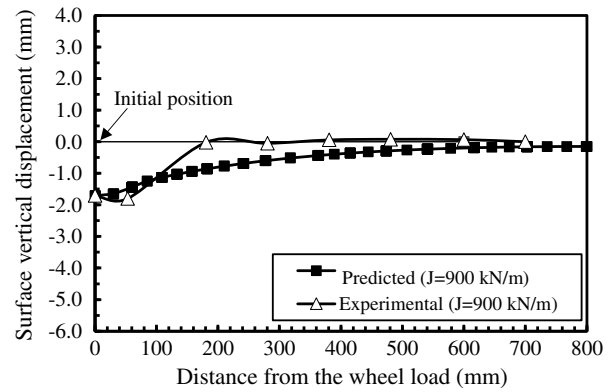
Fig. 4. Comparison of experimental and predicted surface vertical displacements.

rutting profiles reported by Correia and Zornberg (2016), after an initial intense rate of deformation (up to 20,000 load cycles), AC deformation stabilized throughout the test (up to 100,000 load cycles), resulting in a uniform deformation over time. Saevarsdottir (2014) found a similar rutting development behavior as part of a comparison of finite-element model results and results from laboratory large-scale pavement sections. In those evaluations as well, the model did not capture an excessive amount of rutting in the initial stages of the test. Even though the model used in this research did not capture all aspects of AC layer long-term performance, the numerical predictions show good correlation in terms of maximum surface vertical displacements.

Fig. 5 shows the horizontal strain distribution along the geogrid reinforcement, as obtained in the experimental program and in the numerical predictions, conducted using the initial stiffness (J) of the actual geogrid ($J = 900$ kN/m). The numerical model captured the same trend in strain distribution as obtained in the experimental results, in which maximum tensile strains developed near the wheel load, and decreased with increasing distance from the wheel path. However, as with the comparison obtained for vertical displacements, shows that the numerical predictions did not precisely capture the trend observed in the experimental results in the area characterized by upheaval of the AC layer (Fig. 5). Ling and Liu (2003) reported on the limitation of the linear elastic models to reproduce volumetric changes in the AC material and the often nonlinear behavior of geogrids. Still, the model was capable of reproducing the magnitude and location of the maximum strain in the geogrid reinforcement. Furthermore, the numerical prediction
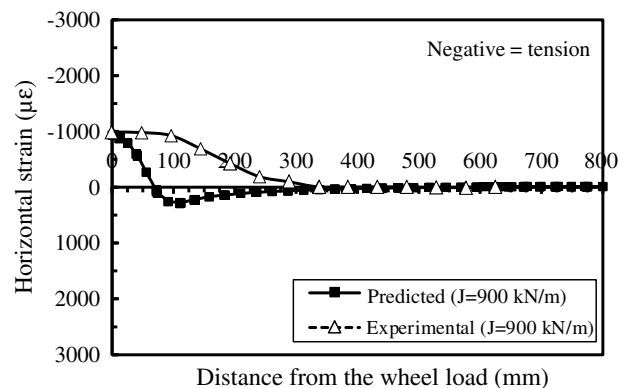
Fig. 5. Comparison of experimental and predicted horizontal strain distribution in geogrid reinforcement.

© ASCE   04018020-4   J. Transp. Eng., Part B: Pavements

J. Transp. Eng., Part B: Pavements, 2018, 144(2): 04018020

Table 2. Range of parameter values adopted in the parametric evaluations

Model	Subgrade Young's modulus (kPa)	J_a	J_b	J_c	J_d
a	6,500	900	2,000	3,000	Unreinforced
b	4,500	900	2,000	3,000	Unreinforced
c	2,500	900	2,000	3,000	Unreinforced
d	1,250	900	2,000	3,000	Unreinforced

was able to properly define the area along which there was no geo-grid mobilization (300 mm from the wheel load). Thus, the finite-element procedures adopted in this research were able to predict the vertical stress distribution and, with reasonable accuracy, the surface vertical displacement profile and geogrid strain distribution obtained from experimental results. Correia (2014) provided similar results of cumulative plastic strains obtained by the transverse ASG installed between AC layers compared with the results presented in the finite-element model (approximately 1,000 $\mu\varepsilon$).

Finite-Element Parametric Evaluation

The finite-element parametric evaluation proposed in this study was conducted using the validated geogrid-reinforced finite-element model focused on assessing the effect of varying the reinforcement and subgrade stiffness. The presence of weak subgrades was represented by adopting a comparatively low Young's modulus for the soil, which is related to low California bearing ratio values. A weak subgrade was used in order to assess the potential of geogrid-reinforced asphalt overlays to enhance the bearing capacity of flexible pavements. Table 2 presents the input parameters adopted to

represent the reinforcement materials and the subgrade. As part of the parametric study, a comparatively thin AC layer involving a 20-mm-thick lower asphalt layer and a 30-mm-thick upper asphalt layer was used in the pavement structure. The simulations were conducted in order to assess the combined effect of varying both the geogrid and subgrade stiffness. The thickness of the base course layer (200 mm) and the subgrade layer (1.0 m) were not changed. The parametric evaluations focused on the effect of stiffness in the geogrid and subgrade materials on the vertical stresses in pavement layers, the lateral strains in the pavement layers, the vertical surface displacements, and the strain distribution in the geogrid installed between asphalt layers.

Fig. 6 shows the results of a parametric evaluation illustrating the effect of geogrid stiffness on the vertical stress distribution in the pavement models. Analyses were conducted using different subgrade conditions characterized by subgrade stiffness values ranging from 1,250 to 6,500 kPa. The predicted vertical stress profiles varied with different subgrade stiffness for reinforced and unreinforced models.

The presence of the geosynthetic reinforcement affected the distribution significantly relative to that observed in the unreinforced model. Specifically, the vertical stresses at the bottom of the AC layers and along the base course were considerably reduced when using reinforcements. In addition, increasing geogrid stiffness values were found to directly affect the stresses transmitted to the base course layer. This behavior was found to be more significant in the case of comparatively weak subgrades [e.g., Fig. 6(d)], in which the reinforcement effect led to more significant improvement.

Fig. 7 presents the vertical profiles of predicted lateral strains profiles, which illustrates the effect of geogrid stiffness on the lateral strain profiles (under wheel load) for different subgrade
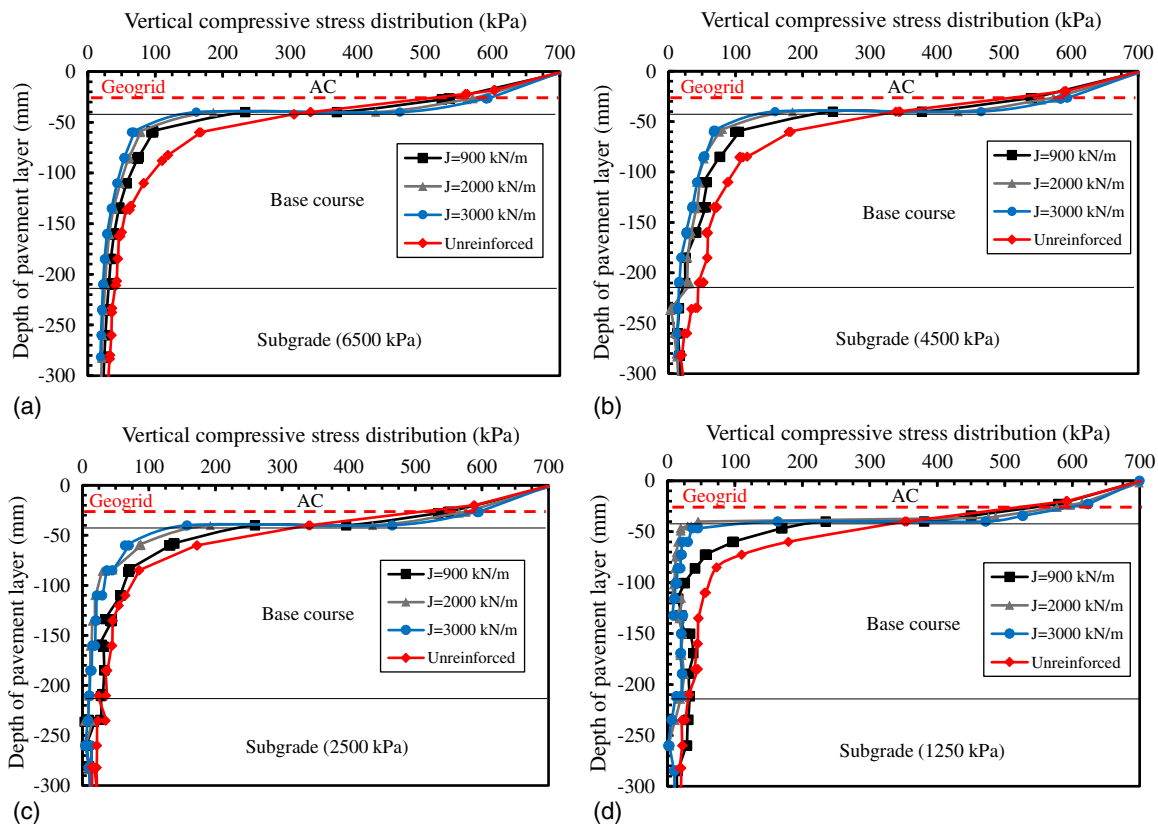
Fig. 6. Effect of geogrid stiffness on the predicted vertical stress profiles for different subgrade stiffnesses: (a) 6,500 kPa; (b) 4,500 kPa; (c) 2,500 kPa; and (d) 1,250 kPa.
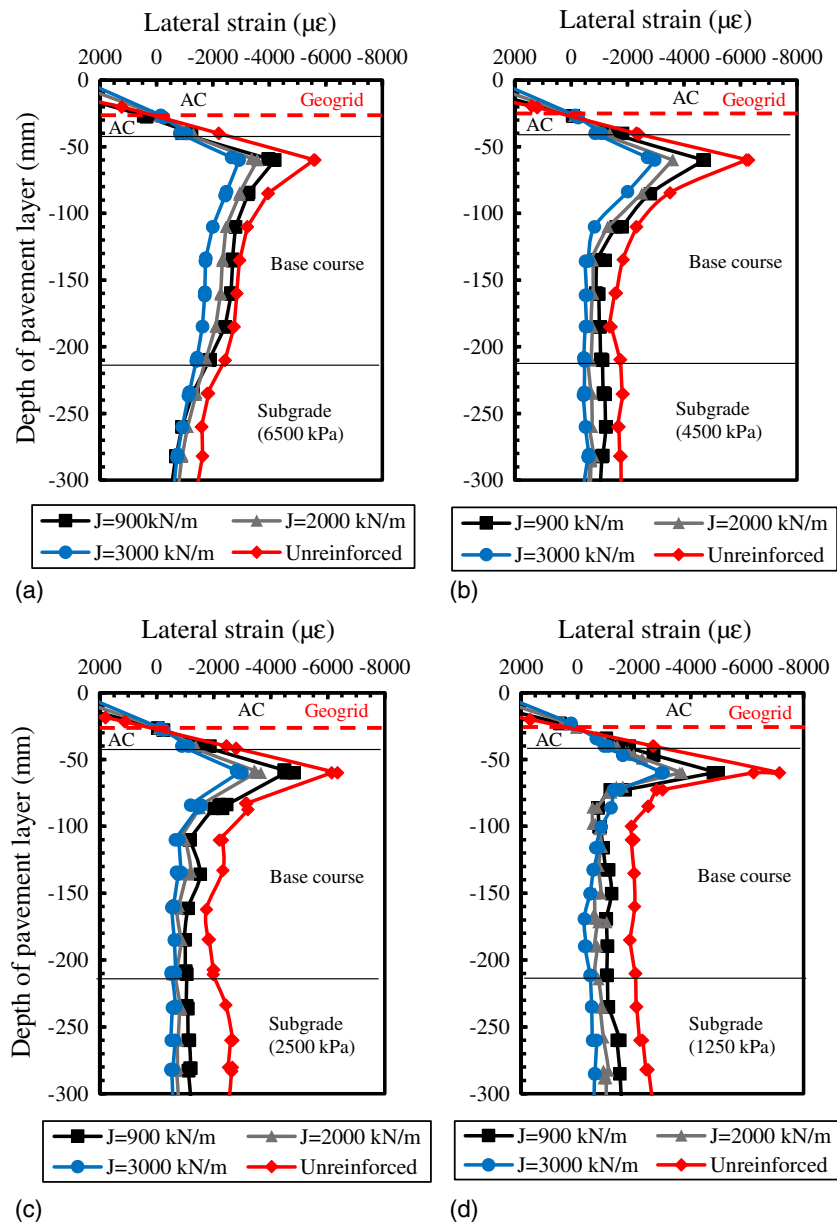
Fig. 7. Effect of geogrid stiffness on the lateral strain profiles for different subgrade stiffnesses: (a) 6,500 kPa; (b) 4,500 kPa; (c) 2,500 kPa; and (d) 1,250 kPa.

stiffness values. The presence of geogrid reinforcements between AC layers was found to lead to a reduction in lateral strains, especially toward the bottom of AC layers and at the top of base course layers. The magnitude of the tensile strains at the bottom of AC layer is particularly relevant in pavement design methods, because these strains are responsible for the development of cracks. The results in Fig. 7 show that, even though the presence of the geogrid reinforcement led to important reductions in the tensile strains of various pavement layers, such reduction was not particularly affected by the magnitude of the geogrid stiffness, at least for the stiffness range considered in this evaluation. These trends are consistent with those reported by Taherkhani and Jalali (2016), who indicated that finite-element predictions of geogrid-reinforced asphalt layers result in tensile strains reductions that were not sensitive to the geosynthetic stiffness. Consequently, the use of high-stiffness geogrids may not result in significant reductions in lateral strains. In addition, the use of geogrid reinforcement inclusion in

the asphalt layers was found to result in reasonably constant lateral strains in pavement layers (for the different subgrade stiffness values considered in this study). On the other hand, the numerical predictions indicate that the level of lateral strains in unreinforced systems increases with decreasing subgrade stiffness.

A reduction in pavement vertical stresses, concurrent with a reduction in lateral strains, was found to result in reductions in pavement vertical deflections. Fig. 8 shows maximum surface vertical displacements directly under the wheel load (rut depth) predicted for different subgrade and geogrid stiffness values. The placement of a geogrid reinforcement at the interface between asphalt layers was found to lead to a reduction in the maximum surface deformations of all reinforced models, as also observed in the experimental laboratory tests. Comparison of the predicted deflections in the reinforced and unreinforced models revealed that the maximum rut depth was reduced by up to 40%, which shows that the geogrid acted as a reinforcement element within the pavement

© ASCE   04018020-6   J. Transp. Eng., Part B: Pavements

J. Transp. Eng., Part B: Pavements, 2018, 144(2): 04018020
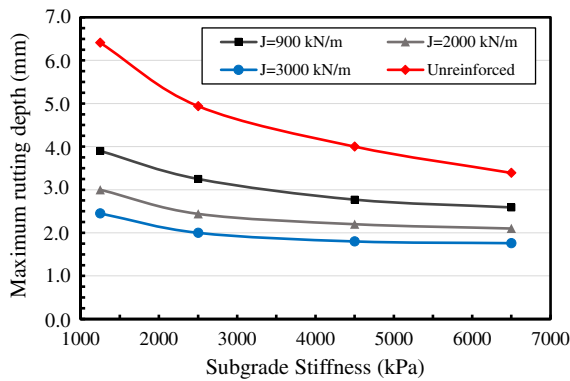
Fig. 8. Maximum rutting depth at asphalt concrete surface for different subgrade stiffnesses.

structure. The improvement was more evident for the case of comparatively weaker subgrade conditions. However, the increase in geogrid stiffness was found not to affect significantly the magnitude of the surface deflection.

In order to gain a better understanding on the geosynthetic reinforcement mechanisms mobilized in a pavement structure with a geogrid installed in the AC layer, the distribution of geogrid strains induced by loading was evaluated for different levels of geogrid stiffness. Fig. 9 shows the predicted horizontal strain distribution at the interface between AC layers (geogrid position) for the range of subgrade and geogrid stiffness values. The magnitude of horizontal strains in the unreinforced model at the interface between AC layers was found to significantly increase with decreasing values of subgrade stiffness (particularly at the wheel path location). On the other hand, the presence of a geogrid between the AC layers resulted in reductions in the tensile strains along the geogrid. Predicted tensile strain distribution and strain magnitude were found to show similar results for the various subgrade stiffness values considered in this study. Under the wheel load, the effect of geogrids stiffness on maximum tensile strains was found to be more prominent for the case of weak subgrades [Figs. 9(c and d)].

Conclusions

This paper presented the results of a two-dimensional finite-element simulations conducted using PLAXIS to analyze geogrid-reinforced asphalt overlays over flexible pavements. The numerical procedures were validated by comparing the experimental results obtained in large-scale accelerated pavement facility with the numerical predictions. A series of finite-element parametric evaluations was conducted with emphasis on the effect of varying geogrid and subgrade stiffness values. Based on the results obtained from this research, the following conclusions can be drawn:

- The finite-element procedures adopted in this research were able to predict the vertical stress distributions in pavement layers and, with reasonable accuracy, the asphalt surface vertical displacements. In addition, it was possible to verify the trends in the geogrid strain distribution and mobilized tension, which were also found to be consistent with experimental results.
- The numerical predictions indicated that an increase in geogrid stiffness results in reduced pavement vertical stresses, especially for wheel load–induced stresses transmitted to the base course layers and top of the subgrade. This indicates that the presence of a geogrid reinforcement within the asphaltic layers can improve the response of the other layers in the pavement system, particularly in the case of comparatively weak subgrades.
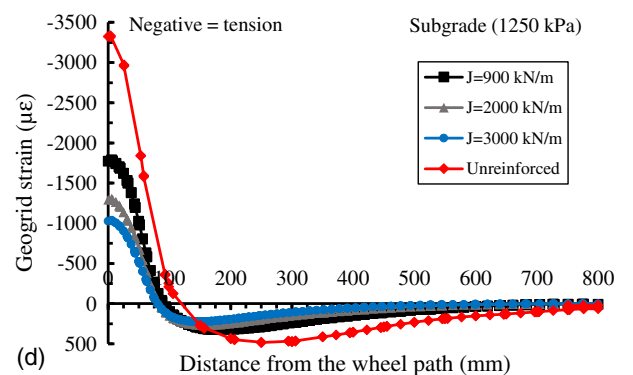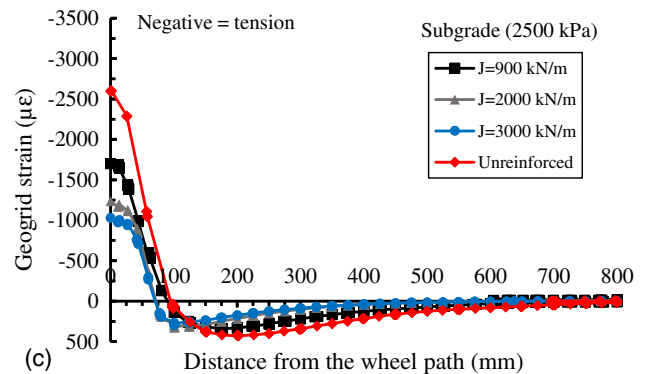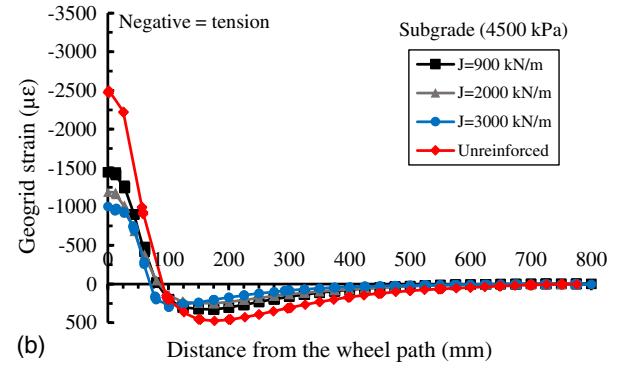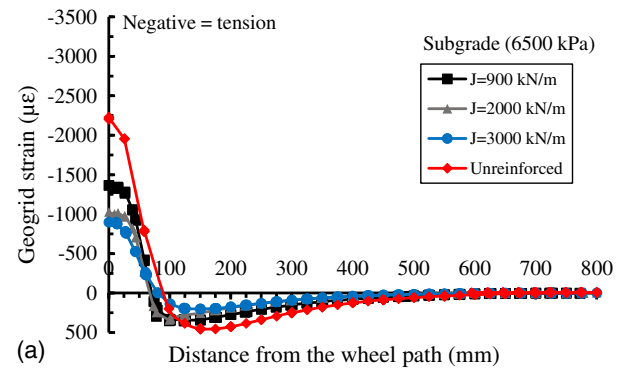
Fig. 9. Horizontal strain distribution at interface of unreinforced and reinforced models for different subgrade stiffnesses: (a) 6,500 kPa; (b) 4,500 kPa; (c) 2,500 kPa; and (d) 1,250 kPa.

- The use of geogrids within the AC layer was found to significantly decrease the magnitude of lateral strains induced over the entire pavement structure. However, the decrease was found not to be particularly affected by the magnitude of the geogrid

© ASCE   04018020-7   J. Transp. Eng., Part B: Pavements

J. Transp. Eng., Part B: Pavements, 2018, 144(2): 04018020

stiffness. The results predicted for the case of reinforced models indicate that the lateral strains at the bottom of the asphalt layer are insensitive to the magnitude of the subgrade stiffness. However, the magnitude of lateral strains was particularly higher in the case of unreinforced than in reinforced systems.

- The asphalt surface vertical displacements were observed to decrease in the geogrid-reinforced models when compared with those in the unreinforced model. The reduction was more significant for the case of comparatively weaker subgrades, although the magnitude of the geogrid stiffness rendered no significant differences in the improved vertical displacements.
- Comparison of the measured and predicted strains along the geogrid reinforcement revealed similar trends in the magnitude and location of strains, regardless of geogrid stiffness. However, the predicted strains were found to be higher for the case of comparatively weaker subgrade conditions.

Overall, the use of finite-element simulations was verified as a versatile tool, with the potential of enhancing the design approaches for reinforced-overlay systems. Results showed that geogrids placed within asphalt layers are able to reduce the load-induced stresses and strains transmitted to pavement layers, even for weak subgrade conditions. This added structural capacity benefit in geogrid-reinforced asphalt layers complements the use of the geosynthetics to minimize reflective cracking.

Acknowledgments

References

Abdesssemed, M., S. Kenai, and A. Bali. 2015. "Experimental and numerical analysis of the behavior of an airport pavement reinforced by geogrids." *Constr. Build. Mater.* 94: 547–554. https://doi.org/10.1016/j.conbuildmat.2015.07.037.

Abu-Farsakh, M., and Q. Chen. 2011. "Evaluation of geogrid base reinforcement in flexible pavement using cyclic plate load testing." *Int. J. Pavement Eng.* 12 (3): 275–288. https://doi.org/10.1080/10298436.2010.549565.

Abu-Farsakh, M. Y., J. Gu, G. Z. Voyiadjis, and Q. Chen. 2014. "Mechanistic–empirical analysis of the results of finite element analysis on flexible pavement with geogrid base reinforcement." *Int. J. Pavement Eng.* 15 (9): 786–798. https://doi.org/10.1080/10298436.2014.893315.

Al-Jumaili, M. A. H.. 2016. "Finite element modelling of asphalt concrete pavement reinforced with geogrid by using 3-D plaxis software." *Int. J. Mater. Chem. Phys.* 2 (2): 62–70.

ASCE. 2017. "Infrastructure report card." Accessed May 10, 2017. http://www.infrastructurereportcard.org/wp-content/uploads/2016/10/2017-Infrastructure-Report-Card.pdf.

ASTM. 2015. *Standard Practice for Classification of Soils and Soil-aggregate Mixtures for Highway Construction Purposes*. ASTM D3282. West Conshohocken, PA: ASTM.

ASTM. 2015. *Standard test method for determining tensile properties of geogrids by the single or multi-rib tensile method*. ASTM D6637. West Conshohocken, PA: ASTM.

Austin, R. A., and A. J. T. Gilchrist. 1996. "Enhanced performance of asphalt pavements using geocomposites." *Geotext. Geomembr.* 14 (3–4): 175–186. https://doi.org/10.1016/0266-1144(96)00007-610.

Brinkgreve, R. B. J., and P. A. Vermeer. 1998. *PLAXIS finite element code for soil and rock analyses*. Rotterdam, Netherlands: A. A. Balkema.

Correia, N. S. 2014. "Performance of flexible pavements enhanced using geogrid-reinforced asphalt overlays." Ph.D. dissertation, Univ. of Sao Paulo.

Correia, N. S., and J. G. Zornberg. 2016. "Mechanical response of flexible pavements enhanced with geogrid-reinforced asphalt overlays." *Geosynthetics Int.* 23 (3): 183–193. https://doi.org/10.1680/jgein.15.00041.

Dondi, G. 1994. "Three-dimensional finite element analysis of a reinforced paved road." In *Proc., 5th Int. Conf. on Geotextiles, Geomembrane and Related Products*, 95–100. Singapore: International Geotextile Society.

Faheem, H., and A. M. Hassan. 2014. "2D Plaxis finite element modeling of asphalt-concrete pavement reinforced with geogrid." *J. Eng. Sci. Assiut Univ. Faculty Eng.* 42 (6): 1336–1348.

Gonzalez-Torre, I., M. A. Calzada-Perez, A. Vega-Zamanillo, and D. Castro-Fresno. 2015. "Experimental study of the behavior of different geosynthetics as anti-reflective cracking systems using a combined-load fatigue test." *Geotextiles Geomembr.* 43 (4): 345–350. https://doi.org/10.1016/j.geotexmem.2015.04.001.

Graziani, A., E. Pasquini, G. Ferrotti, A. Virgili, and F. Canestrari. 2014. "Structural response of grid-reinforced bituminous pavements." *Mater. Struct.* 47 (8): 1391–1408. https://doi.org/10.1617/s11527-014-0255-1.

Khodaii, A., S. Fallah, and F. Moghadas Nejad. 2009. "Effects of geosynthetics on reduction of reflection cracking in asphalt overlays." *Geotextiles Geomembr.* 27 (1): 1–8. https://doi.org/10.1016/j.geotexmem.2008.05.007.

Laurinavičius, A., and R. Oginskas. 2006. "Experimental research on the development of rutting in asphalt concrete pavements reinforced with geosynthetic materials." *J. Civ. Eng. Manage.* 12 (4): 311–317. https://doi.org/10.1080/13923730.2006.9636408.

Ling, H., and H. Liu. 2003. "Finite element studies of asphalt concrete pavement reinforced with geogrid." *J. Eng. Mech.* 129 (7): 801–811. https://doi.org/10.1061/(ASCE)0733-9399(2003)129:7(801).

Ling, H. I., and Z. Liu. 2001. "Performance of geosynthetic-reinforced asphalt pavements." *J. Geotech. Geoenviron. Eng.* 127 (2): 177–184. https://doi.org/10.1061/(ASCE)1090-0241(2001)127:2(177).

Mounes, S. M., M. R. Karim, A. Khodaii, and M. H. Almasi. 2014. "Improving rutting resistance of pavement structures using geosynthetics: An overview." *Sci. World J.* 6. https://doi.org/10.1155/2014/764218.

Nazzal, M., M. Abu-Farsakh, and L. Mohammad. 2010. "Implementation of a critical state two-surface model to evaluate the response of geosynthetic reinforced pavements." *Int. J. Geomech.* 10 (5): 202–212. https://doi.org/10.1061/(ASCE)GM.1943-5622.0000058.

Pandey, S., R. K. Rao, and D. Tiwari. 2012. "Effect of geogrid reinforcement on critical responses of bituminous pavements." In *Proc., 25th ARRB Conf. Shaping the Future: Linking Policy, Research and Outcomes*, 17. Exton, PA: ARRB Group Ltd.

Paterson, W. D. O. 1987. *Road deterioration and maintenance effects: Models for planning and management*. Washington, DC: World Bank.

Perkins, S. W. 2001. *Mechanistic–empirical modeling and design model development of geosynthetic reinforced flexible pavements*. Rep. No. FHWA/MT-01- 002/99160-1A. Helena, Montana: Montana Dept. of transportation.

Rota, V. 2011. "Finite element analysis and laboratory investigation of reinforced road pavements." Ph.D. dissertation, Univ. of Parma.

Saevarsdottir, T. 2014. "Performance modelling of flexible pavements tested in a heavy vehicle simulator." Ph.D. dissertation, Univ. of Iceland.

Siriwardane, H., R. Gondle, and K. Bora. 2010. "Analysis of flexible pavements reinforced with geogrids." *Geotech. Geological Eng.* 28 (3): 287–297. https://doi.org/10.1007/s10706-008-9241-0.

Solaimanian, M. 2013. *Evaluating resistance of hot mix asphalt to reflective cracking using geocomposites*. Rep. No. PSU-2008-04. State College, PA: Pennsylvania State Univ.

Taherkhani, H., and M. Jalali. 2016. "Investigating the performance of geosynthetic-reinforced asphaltic pavement under various axle loads using finite-element method." *Road Mater. Pavement Des.* 18 (5): 1200–1217. https://doi.org/10.1080/14680629.2016.1201525.

© ASCE 04018020-8 J. Transp. Eng., Part B: Pavements

J. Transp. Eng., Part B: Pavements, 2018, 144(2): 04018020